A kinetic model of diamond nucleation and silicon carbide interlayer formation during chemical vapor deposition

Jungheum Yun*, David S. Dandy

Department of Chemical Engineering, Colorado State University, Fort Collins, CO, USA

Abstract

The presence of thin silicon carbide intermediate layers on silicon substrates during nucleation and the early stages of diamond deposition have been frequently reported. It is generally accepted that the intermediate layer is formed by the bulk diffusion of carbon atoms into the silicon carbide layer and the morphology and orientation of the diamond film subsequently grown on the intermediate layer are strongly affected by that layer. While there have been considerable attempts to explain the mechanism for intermediate layer formation, limited quantitative data are available for the layer formation under the operating conditions conducive to diamond nucleation.

This study employs a kinetic model to predict the time evolution of a β-SiC intermediate layer under the operating conditions typical of diamond nucleation in hot filament chemical vapor deposition reactors. The evolution of the layer is calculated by accounting for gas-phase and surface reactions, surface and bulk diffusions, the mechanism for intermediate layer formation, and heterogeneous diamond nucleation kinetics and of its dependence on the operating conditions such as substrate temperature and inlet gas composition. A comparison between the time scales for intermediate layer growth and diamond nuclei growth is also performed. Discrepancies in published adsorption energies of gaseous hydrocarbon precursors on the intermediate layer—ranging from 1.43 to 4.61 eV—are examined to determine the most reasonable value of the adsorption energy consistent with observed saturated thicknesses, 1–10 nm, of the intermediate layer reported in the literature. The operating conditions that lead to intermediate layer growth followed by diamond deposition vs. those that yield heteroepitaxial diamond nucleation without intermediate layer formation are discerned quantitatively. The calculations show that higher adsorption energies, 3.45 and 4.61 eV, lead to larger surface number densities of carbon atoms, lower saturated nucleation densities, and larger intermediate layer thicknesses. The observed saturated thicknesses of the intermediate layer may be reproduced if the true adsorption energy is in the range of 3.7–4.5 eV. The intermediate layer thickness increases by increasing substrate temperature and inlet hydrocarbon concentration and the dependence of the thickness on substrate temperature is especially significant. Heteroepitaxial diamond nucleation without intermediate layer formation reported in experimental results can be readily explained by the significant decrease of the intermediate layer thickness at lower substrate temperatures and at higher diamond nucleation densities. Further, the present model results indicate that the intermediate layer thickness becomes saturated when growing diamond nuclei cover a very small surface area of that layer.
© 2005 Elsevier B.V. All rights reserved.

Keywords: Diamond; Silicon carbide; Chemical vapor deposition; Nucleation; Intermediate layer; Adsorption energy

1. Introduction

Experimental observations [1–41] indicate the presence of an intermediate layer on a non-diamond substrate surface during nucleation and the early stages of diamond deposition in chemical vapor deposition (CVD) processes. It is believed that intermediate layer formation enhances diamond nucleation densities [2,3,42–44] and thus strongly

* Corresponding author. Present address: Power Electronic Research Center, National Institute of Advanced Industrial Science and Technology (AIST), Tsukuba, Ibaraki 305-8568, Japan.

  E-mail address: jungheum.yun@aist.go.jp (J. Yun).

affects the morphology [2,3,42] and orientation [23, 28] of diamond films subsequently grown on the intermediate layer. When silicon is used as a substrate for diamond CVD, investigators [14–41] have reported that silicon carbide is the predominant form of the intermediate layer. The formation of SiC intermediate layers during diamond CVD is also supported by quasi-equilibrium thermodynamic predictions [45,46].

It is generally accepted that the SiC intermediate layer is very thin, often in the range of 1–10 nm [14,16–18,20,30,34,35]. For example, Sun et al. [34] reported the presence of β-SiC intermediate layers between diamond films and Si substrates in hot-filament CVD (HFCVD) reactors under conditions of 0.5 mol% inlet CH_4 in H_2, 75 Torr, filament temperatures between 2473 and 2673 K, and substrate temperatures between 973 and 1273 K. Thin layers of β-SiC, 1–10 nm, were observed in the earliest stages of diamond deposition. Jiang et al. [30] detected an intermediate layer composed of amorphous and crystalline β-SiC, approximately 10 nm thick, at the interface between a diamond film and a Si substrate in a HFCVD reactor under conditions of 1.0 mol% inlet CH_4 in H_2 and substrate temperatures between 973 and 1173 K. Belton et al. [17] observed that a SiC intermediate layer thicker than 9 nm developed before diamond could be detected in a HFCVD system using 0.2 mol% inlet CH_4 in H_2 carrier gas. Stoner et al. [20] reported the formation of amorphous SiC intermediate layers of 1–10 nm thick prior to diamond growth using a microwave plasma-assisted CVD (MW PACVD) reactor. The existence of a SiC intermediate layer, approximately 10 nm thick, was also observed in a diamond growth experiment on a Si substrate using MW PACVD by Meilunas et al. [14]. Jubber and Milne [35] reported 5 nm SiC intermediate layers in MW PACVD of diamond.

A variety of CVD techniques are used in the experimental study of the formation of SiC intermediate layers during diamond CVD. Among these techniques, HFCVD is probably the easiest method to understand experimentally and conceptually, as well as one of the simplest and most reproducible methods for diamond deposition at low pressures. Therefore, HFCVD is often used to investigate the nucleation and subsequent growth of diamond on a variety of substrates [47].

In a typical diamond HFCVD process, a gas mixture containing small amount of CH_4 in an excess of H_2 enters a reactor and flows past a high temperature filament. In the gas phase, CH_4 undergoes pyrolysis reactions leading to a distribution of species that includes carbon atoms, hydrocarbon radicals, and stable hydrocarbon species. Gaseous hydrocarbon species flow toward the hot deposition surface, heated to temperatures between 973 and 1273 K, and impinge on the surface. Some of hydrocarbon species colliding with the surface are adsorbed, while adsorbed hydrocarbon species may desorb back into the gas phase. On the surface, adsorbed carbon atoms diffuse along the surface or into the SiC intermediate layer. Diamond nucleation occurs on the upper surface of the intermediate layer due to the surface diffusion of adsorbed carbon atoms and reactions leading to cluster growth. The bulk diffusion of adsorbed carbon atoms leads to the formation and subsequent growth of the SiC intermediate layer and that layer growth is terminated when the number of adsorbed carbon atoms is saturated to the extent that diamond nuclei form and grow at the expense of intermediate layer formation.

The formation of polycrystalline SiC films by Si out-diffusion from the Si substrate has been also observed by a number of investigators [34,48–60] during SiC carbonization processes. Without introducing Si-bearing precursors to the system, SiC films were deposited on Si substrates using a variety of hydrocarbon species, including CH_4 and C_3H_8, diluted with H_2. The polycrystalline SiC film formed by Si out-diffusion is distinguished from the SiC intermediate layer by its surface roughness, layer thickness, and void formation. With increasing substrate temperature and decreasing inlet hydrocarbon concentration, the SiC film has usually larger saturated thickness, up to hundreds of nanometers, and rougher surface morphology than those of the intermediate layer in a diamond CVD system. Further, the out-diffusion of Si atoms results in the formation of inverted pyramid-like voids in the Si substrate during carbonization. These observations suggest that the polycrystalline SiC film is formed by out-diffusion of Si atoms from the Si substrate and further reaction of Si atoms with hydrocarbon species on the growth surface. The SiC film growth continues until Si atoms can no longer diffuse to the surface through the SiC film at rates that sustain the film growth and then the thickness of the film asymptotes to a saturated value.

However, the presence of polycrystalline SiC films formed by Si out-diffusion is generally observed at higher substrate temperatures than those for SiC intermediate layer growth during diamond CVD. Experimental results indicate that substrate temperatures between 1273 and 1683 K are generally required to grow polycrystalline SiC films by Si out-diffusion. The upper limit on the substrate temperature, 1683 K, is the melting temperature of the Si substrate [61]. Sun et al. [34] conducted an experimental study comparing substrate temperatures for the growth of SiC intermediate layers by C bulk diffusion and polycrystalline SiC films by Si out-diffusion. They observed diamond deposition on very thin SiC intermediate layers at substrate temperatures between 973 and 1273 K. No thin SiC intermediate layer, however, was observed at higher substrate temperatures between 1273 and 1473 K. Instead, only polycrystalline SiC films were grown without further diamond deposition on the SiC films during less than 1 h deposition time. A possible explanation would be that, although the Si out-diffusion is significant if the substrate temperature is relatively high, it is a secondary effect under diamond nucleation conditions. Therefore, although the SiC layer could form either by the bulk diffusion of adsorbed carbon atoms or the Si out-diffusion from the Si substrate, the Si out-diffusion is

negligible at deposition temperatures typical of diamond nucleation in HFCVD reactors.

Accordingly, it appears that when a SiC intermediate layer develops at the interface between a diamond film and a Si substrate it is due to the bulk diffusion of carbon atoms through the intermediate layer toward the Si substrate surface under the operating conditions conducive to diamond nucleation. Therefore, a model of the time evolution of the intermediate layer requires knowledge of the amount of adsorbed carbon atoms available for intermediate layer formation. The amount of adsorbed carbon atoms may be calculated through the consideration of both kinetics of diamond nucleation and intermediate layer formation.

Extensive experimental investigations [14–41] have revealed the existence of SiC intermediate layers on Si substrates during diamond CVD; however, theoretical modeling studies of intermediate layer formation are scarce and the kinetics are not completely understood. Attempts to describe the kinetic aspects of diamond nucleation processes have resulted in the development of models predicting time evolution of the density and rate of diamond nucleation in CVD processes [62–66]. The models captured the critical features associated with diamond nucleation: impingement, adsorption and desorption, surface diffusion, and diamond nucleation. Liu and Dandy [67] developed a theoretical model to capture important physical aspects of diamond nucleation on carbide-forming substrates during the incubation period and the transient nucleation stage in CVD processes. Their model predicted the time evolution of the surface concentration of carbon atoms, as well as the effects of substrate materials such as Si, Ta, W, Mo, Fe, and Ti, surface diffusion, and adsorption state on the diamond nucleation.

Existing diamond nucleation models [62–67] can be applied to investigate the formation of the β-SiC intermediate layer in diamond CVD by using the appropriate kinetic mechanism—one that includes impingement, adsorption and desorption, surface diffusion, and diamond nucleation—associated with diamond nucleation. These models, however, are limited in their ability to reproduce reported experimental observations of intermediate layer formation. These models have been limited by resolving (i) interaction mechanisms of predominant hydrocarbon species with the surface of the intermediate layer, (ii) adsorption energies and bulk diffusion energies, (iii) the bulk diffusion mechanism of adsorbed carbon atoms into the intermediate layer, (iv) the mechanism for intermediate layer formation, (v) effects of deposition parameters on intermediate layer formation, and (vi) influences of the structure of the intermediate layer on diamond nucleation.

The present study constitutes a theoretical examination of important aspects of the formation of the β-SiC intermediate layer between diamond films and Si substrates during nucleation and the early stages of diamond deposition. The purpose of this study is to (i) predict the time evolution

of a β-SiC intermediate layer under the operating conditions conducive to diamond nucleation via HFCVD, (ii) determine the dependence of the time evolution of the layer on operating parameters such as substrate temperature and inlet gas composition, (iii) compare the time scales associated with intermediate layer growth and diamond nuclei growth, (iv) examine discrepancies in published adsorption energies of gaseous hydrocarbon precursors on the β-SiC (100) surface and then determine the most reasonable value of the adsorption energy consistent with published experimental data for intermediate layer thickness, and (v) discern, quantitatively, the operating conditions that lead to intermediate layer growth followed by diamond deposition vs. those that yield heteroepitaxial diamond nucleation without intermediate layer formation.

In the current study, a model is developed to investigate the formation of the β-SiC intermediate layer during nucleation and the early stages of diamond deposition in HFCVD reactors. The model is built on an existing diamond nucleation model dealing with problems related to impingement, adsorption and desorption, surface diffusion, and diamond nucleation. The existing diamond nucleation model is modified to capture mechanisms for both intermediate layer formation and diamond nucleation on the intermediate layer by introducing additional kinetic information such as adsorption energies and sticking coefficients of gaseous hydrocarbon species on the β-SiC (100) surface, bulk diffusion energies and mechanisms of adsorbed carbon atoms through defects of the intermediate layer, and time-dependent growth mechanisms of the intermediate layer and the diamond nucleus.

2. Model description

A kinetic mechanism—including gas-phase and surface reactions, impingement, adsorption and desorption, surface and bulk diffusions, diamond nucleation, and β-SiC intermediate layer formation—is built on an existing diamond nucleation model with detailed information of adsorption energies, bulk diffusion energies, and sticking coefficients. In particular, the near-surface concentrations of gaseous hydrocarbon species are determined under the operating conditions conducive to diamond nucleation in HFCVD reactors. The predominant hydrocarbon species impinge on the surface. The adsorption rates of the hydrocarbon species are determined by the impingement rates and the sticking coefficients of the species on the deposition surface. Desorption of adsorbed hydrocarbon species then occurs with a desorption rate determined by a representative residence time. Hydrogen is sequentially removed from adsorbed hydrocarbon species and adsorbed species decompose to carbon atoms before these atoms diffuse along the surface or into the intermediate layer. In the present model, β-SiC (100) is assumed to be the

intermediate layer and the surface radical sites of the intermediate layer are considered for surface reactions.

The bulk diffusion of adsorbed carbon atoms through the SiC layer leads to continued intermediate layer growth. Initially the surface is (100) silicon after which the adsorbed carbon reacts with the surface to form β-SiC. The adsorbed carbon atoms diffuse to reach the interface between the intermediate layer and the Si substrate and react with Si to form β-SiC. Intermediate layer growth effectively ceases when the surface density of adsorbed carbon atoms is saturated to the extent that diamond nuclei form and grow at the expense of intermediate layer formation. In the current model, rapid reaction occurs at the interface between the SiC intermediate layer and the Si substrate, while the bulk diffusion of adsorbed carbon atoms is slow. The reaction rate coefficient is determined to be larger than the bulk diffusion coefficient by a factor of 10^{21}–10^{14}, depending on substrate temperature in the range of 973–1273 K. Under this circumstance the formation of the β-SiC intermediate layer is controlled by the bulk diffusion rate.

The high lattice mismatch at the interface ($\approx 22\%$) between the β-SiC intermediate layer and the Si substrate promotes dislocations and the spacing between dislocations is in the order of only few lattice constants. As the β-SiC intermediate layer grows, defects develop through the intermediate layer due to the high density of interface dislocations. Of the various defect types, grain boundary defects and lattice vacancy defects are expected to be the primary routes for the bulk diffusion of carbon atoms into the β-SiC intermediate layer [68]. The predicted diffusion rates of carbon atoms through these two types of defects are compared to choose the dominant bulk diffusion route.

The surface diffusion of adsorbed carbon atoms leads to the formation and subsequent growth of diamond nuclei on the upper surface of the evolving β-SiC intermediate layer. During the initial stages of diamond nucleation, the nuclei may either grow or shrink depending on kinetic and thermodynamic conditions. When the number of carbon atoms present in the diamond nucleus exceeds a certain critical number, i, the nucleus is considered to be stable and will continue to grow. A diamond nucleus containing i carbon atoms is referred to as the critical nucleus and all larger nuclei containing at least $i+1$ carbon atoms are referred to as the stable nuclei. The growth of nuclei is the result of the surface diffusion of adsorbed carbon atoms. The surface density of stable nuclei increases with time and eventually reaches a saturation value. The saturated surface density of stable nuclei may be determined by calculating the depletion of adsorbed carbon atoms due to the growth of nuclei existing within the area equal to the square of the average surface diffusion length. With further growth after the saturation value, the stable nucleus size is continuously grown without changing the surface density of stable nuclei and later the surface density decreases due to the coalescence between nuclei. A continuous diamond film is formed on the upper surface of the β-SiC intermediate layer when isolated nuclei grow continuously and coalesce eventually.

A model is developed to predict β-SiC intermediate layer formation and transition to diamond nucleation. In the present study, it is not necessary to observe system up to the point of nuclei coalescence because intermediate layer growth rate is negligible long before coalescence. Because of this the early stages of diamond deposition until growing diamond nanocrystallites cover a small surface area, up to 1% of the overall surface area, of the β-SiC intermediate layer is considered. When growing diamond nuclei cover less than 1% of the surface area of the intermediate layer, it is not unreasonable to assume that the growth of diamond nuclei is in its earliest stages. The β-SiC is considered as the surface material in the present model and thus the model provides a quantitative estimate of the surface adsorption occurring only after a continuous β-SiC layer forms on the Si substrate surface. The surface detachment of diamond nuclei−unstable, critical, and stable nuclei−containing more than one carbon atom is not accounted since desorption energies of these nuclei are expected to be much larger than adsorbed carbon atoms. Further, diamond nuclei are not considered to be mobile [69] and therefore only carbon atoms are assumed to diffuse along the surface to form diamond nuclei.

A set of rate equations, which describes the kinetic behaviors of adsorbed carbon atoms and diamond nuclei, can predict the time evolution of the surface densities of carbon atoms and diamond nuclei on the surface. The time evolution of the surface density of adsorbed carbon atoms is determined by the adsorption rates of gaseous hydrocarbon species, the desorption rates of adsorbed hydrocarbon species, the capture rates of adsorbed carbon atoms by stable nuclei and critical nuclei, and the bulk diffusion rates of carbon atoms into the β-SiC intermediate layer. The time evolution is expressed as

$$\frac{dn_1}{dt} = R_a - \frac{n_1(t)}{\tau_s} - \sigma_x D_s n_1(t) n_x(t)$$
$$- (i+1)\sigma_i D_s n_1(t) n_i(t) - R_d, \qquad (1)$$

where n_1 is the surface density of adsorbed carbon atoms, R_a is the overall adsorption rate of carbon atoms from CH_3 radicals and stable C_2H_2 molecules, τ_s is the residence time of adsorbed hydrocarbon species, D_s is the surface diffusion coefficient of adsorbed carbon atoms, i is the size of critical nuclei, n_i and n_x are the surface number densities of critical and stable nuclei, R_d is the bulk diffusion rate of carbon atoms into the SiC intermediate layer, and σ_i and σ_x, which describe surface diffusion flows of adsorbed carbon atoms to critical and stable nuclei, are the capture numbers and the values are chosen at 4 and 5, respectively [67]. The time evolution of the surface density of stable nuclei is given by

$$\frac{dn_x}{dt} = \sigma_i D_s n_1(t) n_i(t). \qquad (2)$$

The surface density of critical nuclei depends on the number of atoms present in each seed and can be expressed as

$$n_i = \frac{1}{2} n_1 (x - i) \qquad x > i \quad \text{and} \quad n_i = 0 \qquad 1 < x \le i. \tag{3}$$

The critical nucleus size, i, has been predicted to be between 5 and 8 carbon atoms [70]. However, in that study the desorption of diamond clusters was not considered, so the actual critical nucleus size is expected to be slightly larger than the predicted range; therefore, it is assumed in this study that a critical nucleus contains 10 carbon atoms. Not coincidentally, this is also the number of carbon atoms in the diamond structure of the boat–boat conformer of bicyclo-decane. As such, the critical nucleus size is chosen to be 10 carbon atoms and all larger nuclei containing more than 10 carbon atoms are considered to be stable. The average stable nucleus size depends on the surface density of adsorbed carbon atoms,

$$x = \sigma_i D_s \int_0^t n_1(t) dt. \tag{4}$$

The overall adsorption rate of carbon atoms, R_a, is determined by accounting for the impingement rates, R_{imp}, and the sticking coefficients, v, of the predominant gaseous hydrocarbon species, assumed to be CH_3 and C_2H_2 for the operating conditions used in this study, with the surface radical sites, such that

$$R_a = R_{imp} v. \tag{5}$$

The impingement rate, R_{imp}, represents the number of carbon atoms present in the predominant hydrocarbon species colliding with the surface per unit time and area and is given by [67,71]

$$R_{imp} = j \frac{N_A P}{\sqrt{2\pi M R T}} = 3.513 \times 10^{22} j \frac{P}{\sqrt{MT}}, \tag{6}$$

where j is the number of carbon atoms present in the predominant hydrocarbon species, either 1 or 2 in the calculations, N_A is Avogadro's number, P (torr) is the near-surface partial pressures of the hydrocarbon species, M is the molecular weight of the hydrocarbon species, R is the universal gas constant, and T (K) is the gas temperature at the surface, assumed to be same as the substrate temperature.

For a particular set of operating conditions, the near-surface partial pressures of the gaseous hydrocarbon species are computed through numerical solution of the differential equations describing flow, heat, and mass transfer in a pedestal reactor geometry. A stagnation flow program [72], together with Fortran packages called Chemkin-III [73] and Surface Chemkin [74] for analysis of gas-phase and surface chemical kinetics, is used to predict the near-surface composition. Multicomponent transport properties for the gas phase are calculated using a Fortran computer program [75]. The reversible gas-phase reactions used in the present study are based on an established pyrolysis mechanism [76]. The surface reactions in the model incorporate the roles of atomic hydrogen on the activation and termination of the surface radical sites. It is assumed that the rate coefficients of the activation and termination reactions on a carbon-terminated surface are applicable to a SiC surface. Since atomic hydrogen is extremely reactive it is expected that this assumption is reasonable, even though the surfaces are not chemically identical. The rate coefficients are predicted by Battaile et al. [77] for diamond deposition and shown in Table 1.

Sticking coefficient, v, is defined as a probability of a certain reaction process when a given collision occurs. Calculations of the gas-phase composition in the stagnation flow geometry indicate that the near-surface gas-phase concentrations of CH_3 and C_2H_2 are significantly higher than other hydrocarbon species; therefore, these are the only two hydrocarbon species considered as film growth precursors. At $T_s = 1200$ K the sticking coefficients for CH_3 and C_2H_2 are 0.24 [77] and 0.02 [78]. Since no data is available for reactions of gaseous CH_3 and C_2H_2 species with the surface radical sites of β-SiC, the sticking coefficient for CH_3 is for its reaction with carbon surface sites and the sticking coefficient for C_2H_2 is taken from a study of C_2H_2 adsorption on silicon surfaces.

The desorption rate of adsorbed hydrocarbon species is accounted for using the average residence time of each species. The residence time, τ_s, is a measure of how long, on average, an adsorbed hydrocarbon species remain on the surface before desorbing back into the gas phase. This quantity may be calculated as [67,71]

$$\tau_s = \frac{1}{v_a} \exp\left(\frac{E_a}{k T_s}\right), \tag{7}$$

where v_a is the effective surface vibrational frequency of adsorbed species (assumed to be 10^{13} per second in this study [67]), E_a is the adsorption energy, k is Boltzmann's constant, and T_s is the substrate temperature. Since there is uncertainty regarding the actual value of the adsorption energies of CH_3 and C_2H_2 on the β-SiC (100) surface, a range of adsorption energies are selected from the literature for the Si (100) surface [79,80] and the Si-surface of β-SiC (100) [81], as shown in Table 2. These values are tested in the model to determine the most reasonable value of E_a that is consistent with reported experimental measurements for intermediate layer formation. For $T_s = 1200$ K, the residence

Table 1
Simplified surface reaction mechanism for atomic hydrogen adsorption and abstraction on Si surface radical sites[a]

Reaction	A	β	E
SiH (S)+H$\leftrightarrow$Si (S)+H$_2$	1.3×10^{14}	0.0	7300.0
Si (S)+H$\leftrightarrow$SiH (S)	1.0×10^{13}	0.0	0.0

[a] Arrhenius parameters in form $k_i = AT^\beta \exp(-E/RT)$ in units (A in moles, cubic centimeters, and seconds; E in calories per mole). The surface radical site is represented by (S).

Table 2
Adsorption energies and surface residence times of CH_3 and C_2H_2 for Si (100) and β-SiC (100) surface

Adsorbed species	E_a (eV/atom)[a]	τ_s (s)[b]
CH_3	1.43[78]	9.91×10^{-8}
	2.86[79]	1.03×10^{-1}
	3.29[80]	6.58×10^{0}
C_2H_2	1.73[78]	1.80×10^{-6}
	3.45[79]	3.09×10^{1}
	4.61[80]	2.30×10^{6}

[a] The adsorption energy is assumed to be the same as the desorption energy.
[b] The surface residence time is calculated for a substrate temperature of 1200 K.

times determined from the adsorption energies range from 9.9×10^{-8} s for $E_a = 1.43$ eV to 2.3×10^6 s for $E_a = 4.61$ eV, as shown in Table 2. Although the actual residence time may range from below 1 ns to several hours, depending on the adsorption state, adsorption energy, and substrate temperature [67], the predicted value of τ_s corresponding to $E_a = 4.61$ eV is orders of magnitude above what is accepted to be realistic in diamond CVD. However, by considering adsorption energies in the range $1.43 \leq E_a \leq 4.61$ eV and using the present model to calculate the saturated surface density of stable diamond nuclei and the final thickness of the β-SiC intermediate layer, it will be possible to identify the most probable value for E_a.

An adsorbed carbon atom will not necessarily remain on its initial surface site but may diffuse along the surface or into the bulk of the intermediate layer. The surface diffusion coefficient D_s is given by [67,71]

$$D_s = \frac{\alpha v_d}{N_0} \exp\left(-\frac{E_s}{kT_s}\right), \qquad (8)$$

where α is a constant and assumed to be 1/4 for two-dimensional diffusion [82], v^a is the effective vibrational frequency for the surface diffusion of adsorbed carbon atoms and is assumed to be equal to v_d, $N_0 = 1.05 \times 10^{15}$ cm^{-2} is the total surface site density of β-SiC, and E_s is the activation energy for the surface diffusion of adsorbed carbon atoms. The value of E_s is predicted to be between one-sixth and one-half of E_a [83,84]; in the current study the value of $E_a/2$ is used.

Adsorbed carbon atoms diffuse along the surface during their residence time before desorbing. The average surface diffusion length, λ, of adsorbed carbon atoms is given by [71]

$$\lambda = \sqrt{2D_s \tau_s} = \sqrt{\frac{a^2}{4} \exp\left(\frac{E_a}{2kT_s}\right)}, \qquad (9)$$

where the lattice constant of β-SiC is $a = 4.36 \times 10^{-8}$ cm. Using this result the saturated surface density of stable nuclei, N_s, is determined by [85]

$$N_s = \frac{N_0 a^2}{\lambda^2} = 4N_0 \exp\left(-\frac{E_a}{2kT_s}\right), \qquad (10)$$

where the reactive site density, N_0, is $2/a^2$ for a face centered cubic (fcc) lattice structure.

The bulk diffusion of adsorbed carbon atoms occurs through defects such as grain boundaries and lattice vacancies and is expected to be the primary route for the formation and subsequent growth of the β-SiC intermediate layer [68]. The diffusion coefficients associated with grain boundary and lattice vacancy transport are expressed as [68]

$$D_g = 4.44 \times 10^7 \exp\left(-\frac{5.84}{kT_s}\right),$$

$$D_v = 2.62 \times 10^8 \exp\left(-\frac{8.72}{kT_s}\right), \qquad (11)$$

respectively, where the activation energies in the exponents are in electron volt per atom. The pre-exponential constant and activation energy parameters in the expressions in Eq. (11) contain significant uncertainties, roughly 60%. However, the range of bulk diffusion coefficient values resulting from these uncertainties are not considered in the present study; there are no clear data indicating that the expressions in Eq. (11) should be used to obtain more than an order of magnitude estimate for bulk diffusion coefficients. Further, the activation energy for grain boundary diffusion is less than two-third of the corresponding value for lattice vacancy diffusion and as a result the diffusion coefficient for grain boundary transport is predicted to be eleven orders of magnitude greater than that for lattice vacancy at $T_s = 1200$ K. Consequently, grain boundary diffusion is assumed to be the only diffusion mechanism for bulk transport of carbon atoms in the SiC intermediate layer.

Assuming that the grain boundaries are perpendicularly oriented to the surface and that these boundaries are uniformly distributed throughout the bulk phase of the intermediate layer, the bulk diffusion coefficient, D_b, can be approximated as

$$D_b \approx D_g \frac{\delta_b}{l}, \qquad (12)$$

where δ_b is the average width of grain boundaries, assumed to be 5 Å [86,87]. This value is also similar to the lattice constant of β-SiC (100), 4.36 Å. The average distance between individual grain boundaries, l, can be approximated as $l = d/f$, where $d \approx 3.08$ Å is the distance of nearest atoms on the β-SiC (100) face and $f = 0.22$ represents the lattice mismatch between β-SiC and Si.

The bulk diffusion rate R_d of adsorbed carbon atoms into the β-SiC intermediate layer is predicted using Fick's first law of diffusion, assuming the bulk diffusion through a semi-infinite slab [88]

$$R_d = C_s \sqrt{\frac{D_b}{\pi \cdot t}}, \qquad (13)$$

where C_s (atom/cm^3) is the volume concentration of adsorbed carbon atoms in the bulk near the gas–solid

interface and is given by $C_s = n_1/a_C$ [67], where $a_C = 1.54$ Å is the diameter of a carbon atom.

Given that the total number of carbon atoms diffusing into the β-SiC intermediate layer in time t is given by

$$M_t = \int_0^t R_d dt, \qquad (14)$$

the β-SiC intermediate layer thickness, L, at any time t can be calculated as

$$L = \frac{M_t}{C^*} = \frac{2 \cdot n_{1,s}}{a_C \cdot C^*} \sqrt{\frac{D_b \cdot t}{\pi}}, \qquad (15)$$

where $C^* = 4.83 \times 10^{22}$ C atom/cm^3 is the volume of carbon atoms necessary to form a stoichiometric β-SiC intermediate layer and $n_{1,s}$ is the surface density of adsorbed carbon atoms chosen at the saturation value of the surface density of stable nuclei, $n_1 = n_{1,s}$ and $n_x = N_s$ at $t = t_s$. When the surface diffusion length is of the same order of magnitude as the average distance between clusters and is decreased as the cluster size increases, the surface density of adsorbed carbon atoms is monotonously decreased as the cluster size increases after $t = t_s$ until nuclei coalesce each other. Nevertheless, since the nucleation regime terminates well before the onset of coalescence and the stable nuclei occupied very small portion of the surface during the nucleation, the dependence of the surface diffusion length on the cluster size increase is so small that n_1 is not appreciably changed during the nucleation and the intermediate layer growth concerned in this study.

There is evidence in support of the information that the intermediate layer growth effectively ceases during the early stages of diamond deposition [14,17,20,34]. To confirm that the information is reasonable, calculations are performed under different conditions to compare the time scales associated with intermediate layer growth and diamond nuclei growth. The time scale for diamond nuclei growth is represented by the time evolution of the surface area, S, covered by growing diamond nuclei. The van der Drift model [89,90] is applied to predict the S value. The time evolution of S is determined from the lateral growth velocity of diamond nuclei, V_l, the average distance between individual diamond nucleus, d_0, and the saturated surface density of stable nuclei. A value for V_l is calculated from a model based on the growth rate parameter, $\alpha_{3D} = \sqrt{3}\, V_{100}/V_{111}$, where V_{100} and V_{111} are the growth velocities of the {100} and {111} faces on a diamond nucleus. In typical diamond CVD processes two crystal faces, {111} and {100}, are commonly observed, whereas the faster growing {110} face is not as prevalent. Thus, the nuclei evolution model can be simplified to the growth of two-dimensional nuclei, where the appropriate growth rate parameter, α_{2D}, is related to the ratio of the growth velocities of the {10} and {11} faces on a diamond seed. The two-dimensional parameter is defined as $\alpha_{2D} = \sqrt{2}\, V_{10}/V_{11}$, where V_{10} and V_{11} are the growth velocities of the {10} and {11} faces

[91]. Once V_{11} is calculated from known values of α_{2D} and V_{10} corresponding to specific growth conditions, the average growth velocity onto the lateral surface, V_l, is determined to be at same magnitude of V_{10}. Choosing the operating parameters such as $T_s = 1200$ K and the inlet mole fraction of CH$_4$ in H$_2$ $X_{CH_4} = 0.02$, the values of the growth velocity of the {10} face, V_{10}, [77] and the two-dimensional growth parameter, α_{2D}, [90] are adopted from the literature. The average distance between individual diamond nucleus, d_0, is calculated from the saturated surface density of stable nuclei N_s.

3. Results and discussion

For the calculations carried out in this study, the operating conditions typical of diamond nucleation in HFCVD reactors are chosen as follows: reactor pressure $P = 50$ Torr, inlet gas flow rate $U_\infty = 300$ sccm, distance from the substrate surface to the filament $D = 0.5$ cm, and filament temperature $T_f = 2500$ K. Calculations are performed for two different substrate temperatures, $T_s = 1000$ and 1200 K. The operating conditions used in the present calculations are summarized in Table 3. Calculations are also performed for different inlet compositions by varying the inlet mole fraction of CH$_4$ in H$_2$, X_{CH_4}, from 0.005 to 0.04. To obtain an estimate of the degree of heterogeneous H$_2$ dissociation on the surface of the 2500 K filament, a linear filament poisoning model is applied [92].

The mole fractions of the predominant gaseous hydrocarbon species at the deposition surface and the overall adsorption rate of carbon atoms are evaluated for different substrate temperatures and inlet compositions, as listed in Table 4. The mole fractions are determined by computing the gas-phase velocity, temperature, and concentration profiles in an idealized stagnation flow geometry [92]. It is predicted that hydrocarbon species such as CH$_3$ and C$_2$H$_2$ are present at the surface in sufficiently large concentrations to be considered as the predominant precursor species. For example, when the near-surface concentrations of CH$_3$ and C$_2$H$_2$ are compared to the other CH$_x$ and C$_2$H$_y$ hydrocarbon species, the concentrations of these other species are always at least an order of magnitude lower than those of CH$_3$ and C$_2$H$_2$. Because of this observation, hydrocarbon species

Table 3
Operating conditions used in the present calculations

Total gas pressure	50 Torr		
Inlet gas velocity	1.0 cm/s		
Filament temperature	2500 K		
Distance from substrate surface to filament	0.5 cm		
Substrate temperature	1000, 1200K		
Inlet mole fraction	CH$_4$	H$_2$	H
	0.005	0.906	0.089
	0.010	0.935	0.055
	0.020	0.949	0.031
	0.040	0.943	0.017

Table 4
Calculated mole fractions of predominant gaseous hydrocarbon species at the deposition surface and overall absorption rate of carbon atoms

Operating parameters	Mole fraction		Overall adsorption rate R_a
Substrate temperature, K	CH_3	C_2H_2	
1000	1.34×10^{-3}	5.47×10^{-3}	6.34×10^{18} cm^{-2}
1200	1.22×10^{-3}	4.64×10^{-3}	5.15×10^{18} cm^{-2}
Inlet mole fraction of CH_4	CH_3	C_2H_2	
0.005	8.61×10^{-4}	2.59×10^{-3}	3.37×10^{18} cm^{-2}
0.02	1.62×10^{-3}	6.63×10^{-3}	7.01×10^{18} cm^{-2}
0.04	1.92×10^{-3}	6.67×10^{-3}	7.86×10^{18} cm^{-2}

other than CH_3 and C_2H_2 are not considered as growth precursors in this study. Once the total impingement rate of carbon atoms is known from Eq. (6), the overall adsorption rate may be calculated using Eq. (5).

The saturated surface density of stable nuclei, N_s, is calculated for different substrate temperatures, T_s, and adsorption energies, E_a, using Eq. (10) as shown in Fig. 1. Two substrate temperatures, 1000 and 1200 K, are chosen to quantitatively probe the sensitivity of N_s to this parameter. For a specific substrate temperature, N_s decreases extensively as E_a is increased from 1.43 to 4.61 eV. For example, for $T_s = 1200$ K N_s is predicted to be 4.2×10^{12} cm^{-2} for $E_a = 1.43$ eV, but the nuclei density drops almost seven orders of magnitude to 8.8×10^5 cm^{-2} when $E_a = 4.61$ eV. As the substrate temperature is decreased from 1200 to 1000 K, N_s also decreases because the surface diffusion rate of adsorbed carbon atoms is slower at lower temperature. The saturated nucleation density of diamond obtained on untreated Si substrates is typically observed to be bellow $\sim 10^6$ cm^{-2} in diamond nucleation studies using HFCVD reactors [93]. For this upper bound of $N_s = 10^6$ cm^{-2}, the corresponding adsorption energy is evaluated to be 4.6 eV by Eq. (10) at 1200 K. However, it has also been observed in HFCVD experiments that the nucleation density of diamond monotonically increases with temperature until it reaches a maximum value at 1223 K substrate temperature and then decreases with further increases in the substrate temperature [94]. The inverse relationship between nucleation density and temperature for $T_s > 1223$ K cannot be captured by the current model. In particular, the model is not applied to substrate temperatures above 1200 K because at these higher temperatures other carbon phases may appear and the model is only set up for the diamond phase.

Fig. 2 shows the saturated surface density of adsorbed carbon atoms, $n_{1,s}$, and the time required to reach saturation, t_s, for different substrate temperatures and adsorption energies. Considering the uncertainty in the value of the adsorption energy, three different published adsorption energies for C_2H_2 are used in the calculations. For a specific adsorption energy, $n_{1,s}$ and t_s decrease extensively as T_s is increased from 1000 to 1200 K. At the higher substrate temperature, a larger surface diffusion rate, a larger saturated

surface density of stable nuclei, and a shorter residence time are all predicted. The value of N_s is principally affected by the surface diffusion rate and is expected to increase when the surface diffusion rate increases for a specific E_a. The value of $n_{1,s}$ increases with increasing E_a for constant operating conditions because longer residence times and lower surface diffusion rates are expected at larger E_a values and these lead to larger $n_{1,s}$ values. The time required to reach saturation is very short ($<10^{-2}$ s) relative to the total growth time of the intermediate layer and larger saturated surface density of stable nuclei leads to longer t_s. Further, the time depends on surface diffusion rate, residence time, saturated nucleation density, and operating conditions. However, the values of $n_{1,s}$ and t_s are not affected appreciably by changes in the inlet mole fraction of CH_4, as demonstrated in Fig. 2(c) and (d).

The time evolution of the intermediate layer thickness, L, is determined for the three different published E_a values for C_2H_2, as shown in Fig. 3. The calculations indicate that a higher adsorption energy leads to a thicker intermediate layer due to a larger $n_{1,s}$ at the upper surface of the intermediate layer. For $T_s = 1200$ K and $X_{CH_4} = 0.01$, the intermediate layer reaches thickness of 10.5, 0.6, and 0.0006 nm for $E_a = 4.61$, 3.45, and 1.73 eV, respectively, during a 1 h deposition time. There is evidence to support that the β-SiC intermediate layer thickness becomes saturated during nucleation and the early stages of diamond deposition [14,17,20,34]. Regarding the actual duration of intermediate layer growth, reported times vary from minutes to hours and this wide range is attributed to implementation of different surface pretreatment methods and operating conditions. For example, Stoner et al. [20] measured the growth time of an intermediate layer in MW PACVD using X-ray photoelectron spectroscopy (XPS). The data indicated that the intermediate layer thickness saturated after 1 h and did so before significant diamond nucleation could be detected.
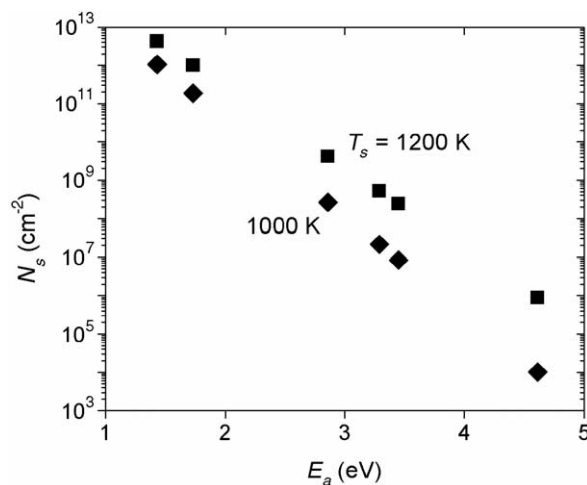

Fig. 1. Saturated surface density of stable diamond nuclei, N_s, for different adsorption energies $E_a = 1.43 - 4.61$ eV and substrate temperatures $T_s = 1000$ and 1200 K.
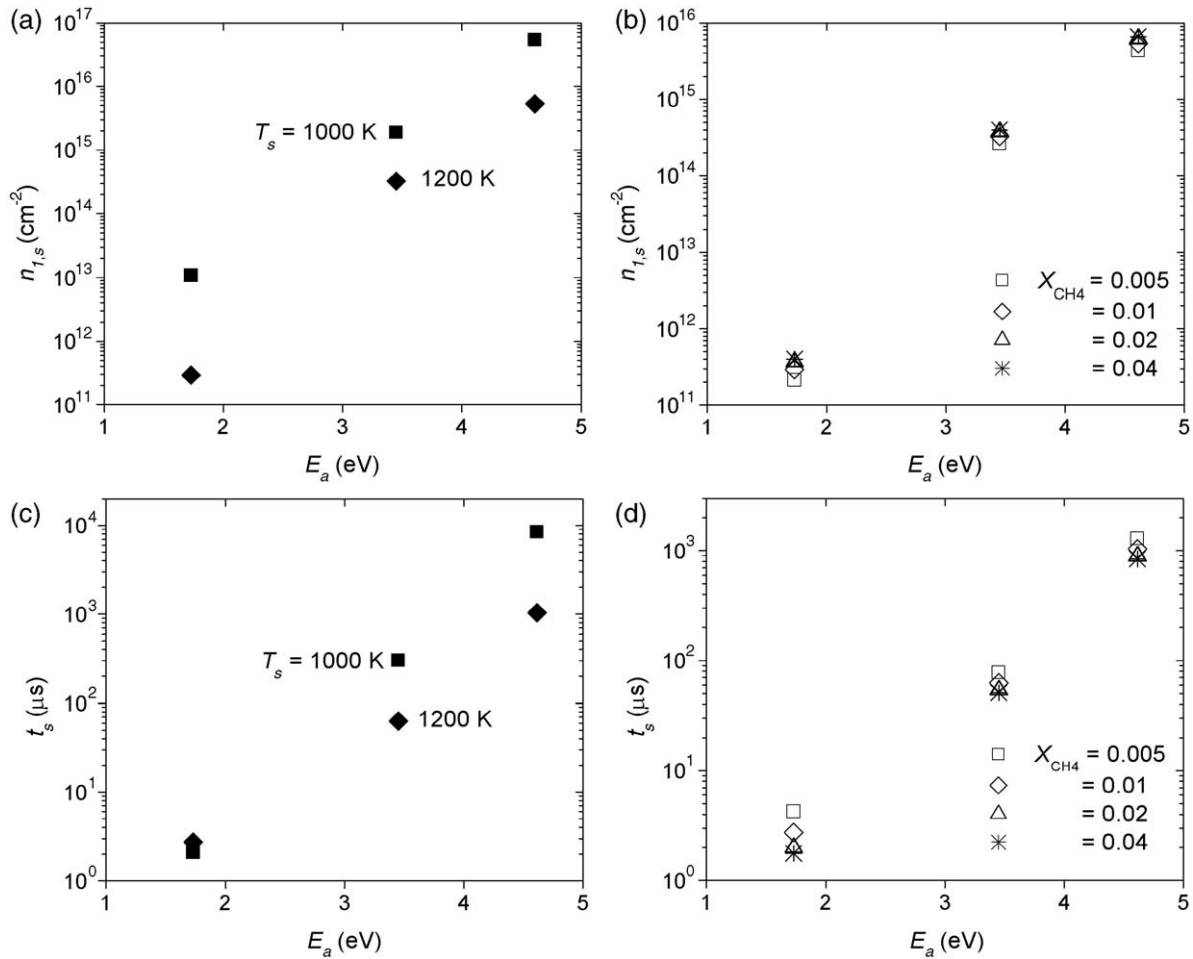
Fig. 2. Saturated surface density of adsorbed carbon atoms, $n_{1,s}$, and time required to reach saturation, t_s, for different values of T_s, X_{CH_4}, and E_a. Figures are (a) $n_{1,s}$ vs. E_a for $T_s = 1000$ and 1200 K, (b) $n_{1,s}$ vs. E_a for $X_{CH_4} = 0.005$, 0.01, 0.02, and 0.04, (c) t_s vs. E_a for $T_s = 1000$ and 1200 K, and (d) t_s vs. E_a for $X_{CH_4} = 0.005$, 0.01, 0.02, and 0.04.

Belton et al. [17] also used XPS to monitor interlayer growth in a HFCVD reactor and they observed a continuous increase in intermediate layer thickness for deposition times

Fig. 3. Time evolution of the intermediate layer for $E_a = 1.73$, 3.45, and 4.61 eV during a 1 h deposition time. Operating conditions are $T_s = 1200$ K and $X_{CH_4} = 0.01$.

up to 4.5 h. However, Meilunas et al. [14] reported that the intermediate layer thickness reached 10 nm after 5 min, while diamond nanocrystallites were observed on the upper surface of the intermediate layer after 1 min. These disparate values for the saturation time of the intermediate layer thickness led to the choice of an intermediate value of 1 h in the present study. Based on the studies indicated above, a time of 1 h would appear reasonable for a bare silicon substrate with little or no pretreatment.
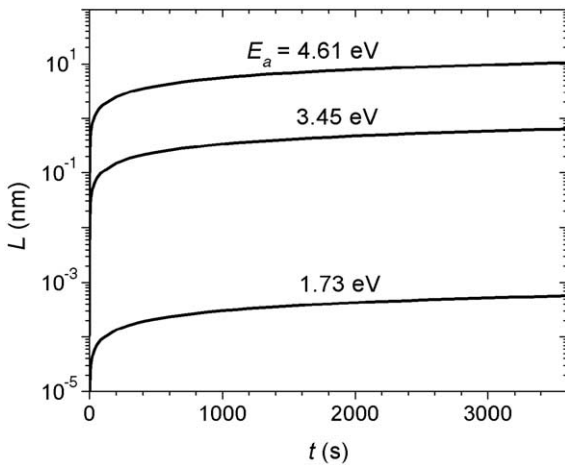
For $E_a = 1.73$ eV, the bulk diffusion rate of adsorbed carbon atoms is not sufficient to initiate the formation of a β-SiC monolayer during a 1 h deposition time. As E_a increases it is calculated that the thickness of the intermediate layer increases significantly. For $E_a = 3.45$ eV, however, the intermediate layer thickness is much larger than for $E_a = 1.73$ eV and the thickness does not reach 1 nm during a 1 h deposition time. When E_a is further increased to 4.61 eV, the intermediate layer thickness is predicted to be 1 nm within 33 s and readily reaches 10.5 nm during a simulated 1 h deposition time.

Figs. 4 and 5 show the dependence of the time evolution of the intermediate layer on the substrate temperature and
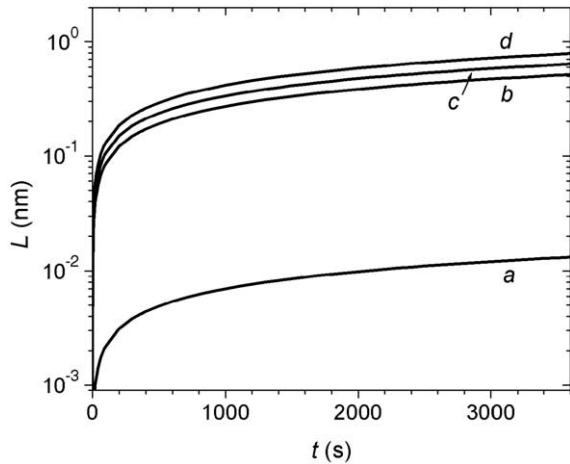
Fig. 4. Dependence of the time evolution of the intermediate layer on T_s and X_{CH_4} for E_a=3.45 eV during a 1 h deposition time. Operating conditions are (a) T_s=1000 K and X_{CH_4}=0.01, (b) T_s=1200 K and X_{CH_4}=0.005, (c) T_s=1200 K and X_{CH_4}=0.01, and (d) T_s=1200 K and X_{CH_4}=0.04.

the inlet gas composition for two different E_a values, 3.45 and 4.61 eV. As may be inferred using Eq. (11), the intermediate layer thickness is strongly dependent on substrate temperature for both values of E_a due to a large increase in the bulk diffusion coefficient for carbon diffusion into the intermediate layer. When T_s increases from 1000 to 1200 K, the thickness increases 48 times for E_a=3.54 eV and 28 times for E_a=4.61 eV during a 1 h deposition time. As X_{CH_4} is raised from 0.005 to 0.04 for a constant 1200 K substrate temperature, the thickness increases from 0.52 to 0.79 nm for E_a=3.54 eV and from 8.53 to 13.03 nm for E_a=4.61 eV for a 1 h deposition time. Further, at the higher substrate temperature (1200 K) and inlet CH$_4$ mole fractions (0.02–0.04) the intermediate layer thickness reaches 1 nm within 24 s for E_a=4.61 eV. However, the calculated thickness decreases considerably at lower substrate temperatures and higher diamond nucleation densities and this result may readily explain direct hetero-
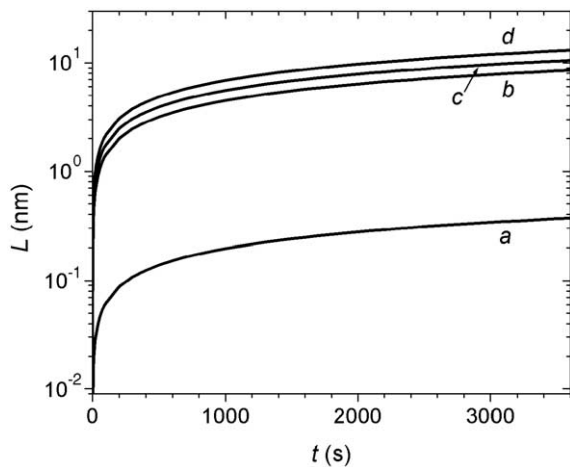
epitaxial diamond nucleation on the Si substrate surface without intermediate layer formation.

The time evolution of surface area, S, covered by growing diamond nuclei is determined from the lateral growth velocity, V_l, of diamond nuclei and the average initial distance, d_0, between individual diamond nuclei for the given N_s. The values of V_l and d_0 are estimated by determining the two-dimensional growth parameters, α_{2D}, and the growth velocity of the {10} crystal face, V_{10}. For T_s=1200 K and X_{CH_4}=0.02, a value for the growth velocity, V_{10}=0.5 μm/h, is adopted from the literature [77]. The value for the two-dimensional growth parameter, α_{2D}=1.86, is also obtained from the literature [90] for the same operating parameters. For this value of V_{10}, the calculated lateral growth velocity of diamond nuclei is V_l=0.27 μm/h. Then, for the values of α_{2D} and V_{10} indicated above, the saturated surface number densities of stable nuclei, N_s=9.9 × 10^{11}, 2.4 × 10^8, and 8.8 × 10^5 cm^{-2}, corresponding to E_a=1.73, 3.45, and 4.61 eV, respectively, may be used to calculate average initial distance between individual stable nuclei. For the three different adsorption energies E_a=1.73, 3.45, and 4.61 eV, the distances are d_0=1 × 10^{-6}, 6.5 × 10^{-5}, and 1.1 × 10^{-3} cm, respectively.

Fig. 6 shows the competition in rates associated with intermediate layer growth and surface coverage of growing diamond nuclei. The time evolution of the intermediate layer is determined assuming low surface area covered by diamond nuclei (≤1% surface area). For T_s=1200 K and X_{CH_4}=0.02, the time required to obtain the point that diamond nuclei cover 1% surface area is calculated to be 7.2 and 119.1 min for E_a=3.45 and 4.61 eV, respectively. At these times, the calculated intermediate layer thickness is 0.26 and 17.3 nm for E_a=3.45 and 4.61 eV, respectively, as shown in Fig. 6. The time evolution of the surface coverage determined for E_a=1.73 eV is distinctly different than for the two higher E_a values and at the lowest adsorption energy it is predicted that the diamond nuclei completely cover the

Fig. 5. Dependence of the time evolution of the intermediate layer on T_s and X_{CH_4} for E_a=4.61 eV during a 1 h deposition time corresponding to the operating conditions described in Fig. 4.
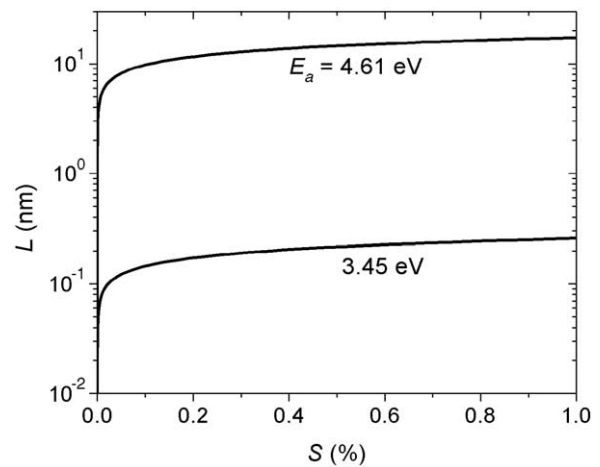

Fig. 6. Competition in rates associated with intermediate layer growth and surface coverage of growing diamond nuclei for E_a=3.45 and 4.61 eV. Operating conditions are T_s=1200 K and X_{CH_4}=0.02.

intermediate layer within the first minute. However, such rapid nuclei growth has not been reported.

Comparing the present model results against a number of experimental studies [14,16–18,20,30,34,35], the reported range for the saturated thickness of the β-SiC intermediate layer, 1–10 nm, are reproduced by the present model if E_a is chosen to be in the range of 3.7–4.5 eV. The present model results also indicate that the β-SiC intermediate layer reaches its saturated thickness during the early stages of diamond deposition and that this saturated thickness is reached before the growing diamond nuclei cover more than approximately 1% of the intermediate layer surface. Because of this, it is possible to predict the saturated intermediate layer thickness as a function of the operating conditions without having to also consider the presence of the diamond nuclei on the upper surface of the intermediate layer.

4. Conclusion

In the present study, a model incorporating gas-phase and surface reactions, surface and bulk diffusion, and heterogeneous diamond nucleation kinetics is applied to predict the time evolution of a β-SiC intermediate layer during the nucleation and the early growth stages of diamond growth under the operating conditions typical of diamond nucleation in HFCVD reactors. The model also quantifies the dependence of the time evolution of the layer on operating parameters such as substrate temperature and inlet gas composition. The time scales associated with diamond nuclei growth and intermediate layer growth are compared by calculating the rate competition associated with intermediate layer growth and surface coverage of growing diamond nuclei. Different published adsorption energies of gaseous hydrocarbon species on the surface of the intermediate layer—ranging from 1.43 to 4.61 eV—are tested to determine an adsorption energy value consistent with the saturation times and final thicknesses (1–10 nm) reported in the literature. Moreover, the operating conditions that typically lead to intermediate layer formation prior to diamond deposition are compared with those conditions that yield heteroepitaxial diamond nucleation without intermediate layer formation.

The present model results reveal that higher adsorption energies—3.45 and 4.61 eV—lead to larger surface concentrations of carbon atoms, lower saturated nucleation densities, and, therefore, larger β-SiC intermediate layer thicknesses. The saturated nucleation density approximated for an adsorption energy of 4.61 eV is typically below 10^6 cm^{-2}, which is in agreement with the nuclei density values reported in the literature. For operating parameters typical of diamond nucleation in HFCVD reactors, $T_s = 1200$ K and $X_{CH_4} = 0.01$, the calculated intermediate layer thickness for $E_a = 4.61$ eV reaches 1 nm within 33 s and 10.5 nm during a 1 h deposition time. However, for $E_a = 3.45$ eV, the intermediate layer thickness is much less than for $E_a = 4.61$ eV and does not reach 1 nm during the same 1 deposition time. The intermediate layer thickness increases at higher substrate temperatures and higher inlet hydrocarbon concentrations. The intermediate layer thickness dependence on substrate temperature is significant due to large increases in the magnitude of the bulk diffusion coefficient for carbon diffusion into the intermediate layer with increasing substrate temperature. The calculations of the rate competition associated with intermediate layer growth and surface coverage of growing diamond nuclei reveal that the intermediate layer thickness becomes saturated at the higher adsorption energies when growing diamond nuclei cover a very small fraction of the upper surface of the intermediate layer. Comparing these calculated results to the literature, the reported saturated thickness of the β-SiC intermediate layer, 1–10 nm, is predicted by the model if the true adsorption energy is in the range of 3.7–4.5 eV. Further, the significant decrease in the intermediate layer thickness at lower substrate temperatures and at higher diamond nucleation densities may provide the explanation for direct heteroepitaxial diamond nucleation on the Si substrate surface without intermediate layer formation.

References

[1] J. Singh, J. Mater. Sci. 29 (1994) 2761.
[2] K.V. Ravi, C.A. Koch, Appl. Phys. Lett. 57 (1990) 348.
[3] K.V. Ravi, J. Mater. Res. 7 (1992) 384.
[4] C. Trevor, D. Cherns, P. Southworth, in: F.J. Humphreys (Ed.), Proceedings of Institute Physics, Electron Microscopy and Analysis Group Conference, IOP, Bristol, UK, 1991, p. 275.
[5] J.J. Dubray, C.G. Pantano, M. Meloncelli, E. Bertran, J. Vac. Sci. Technol., A, Vac. Surf. Films 9 (1991) 3012.
[6] K. Tamaki, Y. Watanabe, Y. Nakamura, S. Hirayama, Thin Solid Films 236 (1993) 115.
[7] P.N. Barnes, R.L.C. Wu, Appl. Phys. Lett. 62 (1993) 37.
[8] R. Csencsits, J. Rankin, R.E. Boekenhauer, M.K. Kundmann, B.W. Sheldon, in: H.A. Atwater, E. Chason, M.H. Grabow, M.G. Lagally (Eds.), Evolution of Surface and Thin Film Microstructure Symposium, M.R.S., Pittsburgh, PA, 1993, p. 695.
[9] A.A. Smolin, S.M. Pimenov, V.G. Ralchenko, T.V. Kononenko, V.I. Konov, E.N. Loubnin, Diam. Films Technol. 3 (1993) 1.
[10] D.N. Belton, S.J. Schmieg, Thin Solid Films 212 (1992) 68.
[11] T.P. Ong, F. Xiong, R.P.H. Chang, C.W. White, J. Mater. Res. 7 (1992) 2429.
[12] W.R.L. Lambrecht, C.H. Lee, B. Segall, J.C. Angus, Z. Li, M. Sunkara, Nature 364 (1993) 607.
[13] X. Peng, H. Li, Mater. Lett. 17 (1993) 223.
[14] R. Meilunas, M.S. Wong, K.C. Sheng, R.P.H. Chang, R.P. VanDuyne, Appl. Phys. Lett. 54 (1989) 2204.
[15] A.R. Badzian, T. Badzian, Surf. Coat. Technol. 36 (1988) 283.
[16] B.E. Williams, J.T. Glass, J. Mater. Res. 4 (1989) 373.
[17] D.N. Belton, S.J. Harris, S.J. Schmieg, A.M. Weiner, T.A. Perry, Appl. Phys. Lett. 54 (1989) 416.
[18] B.E. Williams, J.T. Glass, R.F. Davis, K. Kobashi, J. Cryst. Growth 99 (1990) 1168.
[19] S. Yugo, T. Kimura, T. Muto, Vacuum 41 (1990) 1364.
[20] B.R. Stoner, G.H.M. Ma, S.D. Wolter, J.T. Glass, Phys. Rev., B 45 (1992) 11067.

[21] S.D. Wolter, B.R. Stoner, G.H.M. Ma, J.T. Glass, in: C.L. Renschler, J.J. Pouch, D.M. Cox (Eds.), Novel Forms of Carbon Symposium, M.R.S., Pittsburgh, PA, 1992, p. 347.

[22] Y.H. Shing, F.S. Pool, D.H. Rich, Thin Solid Films 212 (1992) 150.

[23] B.R. Stoner, S.R. Sahaida, J.P. Bade, P. Southworth, P.J. Ellis, J. Mater. Res. 8 (1993) 1334.

[24] D. Kim, H. Lee, J. Lee, J. Mater. Sci. 28 (1993) 6704.

[25] E.G. Wang, Physica. B 185 (1993) 85.

[26] G.A. Hirata, L. Cota-Araiza, M. Avalos-Borja, M.H. Farias, O. Contreras, Y. Matsumoto, J. Phys. 5 (1993) A305.

[27] K. Kobayashi, N. Mutsukura, Y. Machi, T. Nakano, Diamond Relat. Mater. 2 (1993) 278.

[28] S.D. Wolter, B.R. Stoner, J.T. Glass, P.J. Ellis, D.S. Buhaenko, C.E. Jenkins, P. Southworth, Appl. Phys. Lett. 62 (1993) 1215.

[29] M.C. Polo, J. Cifre, J. Esteve, Diamond Relat. Mater. 3 (1994) 492.

[30] N. Jiang, B.W. Sun, Z. Zhang, Z. Lin, J. Mater. Res. 9 (1994) 2695.

[31] S.D. Wolter, J.T. Glass, B.R. Stoner, J. Appl. Phys. 77 (1995) 5119.

[32] T. Suesada, N. Nakamura, H. Nagasawa, H. Kawarada, Jpn. J. Appl. Phys. 34 (1995) 4898.

[33] Y. Ma, T. Tsurumi, N. Shinoda, O. Fukunaga, Diamond Relat. Mater. 4 (1995) 1325.

[34] Z. Sun, Y. Sun, X. Wang, Z. Zheng, Mater. Sci. Eng., B, Solid-state Mater. Adv. Technol. 34 (1995) L13.

[35] G. Jubber, D.K. Milne, Phys. Status Solidi, Appl. Res. 154 (1996) 185.

[36] W. Kulisch, L. Ackermann, B. Sobisch, Phys. Status Solidi, Appl. Res. 154 (1996) 155.

[37] E.J. Corat, N.G. Ferreira, V.J. Trava-Airoldi, N.F. Leite, R.C. Mendes de Barros, K. Iha, J. Mater. Sci. Lett. 16 (1997) 197.

[38] L.C. Nistor, J.V. Landuyt, V.G. Ralchenko, E.D. Obraztsova, A.A. Smolin, Daimond Relat. Mater. 6 (1997) 159.

[39] S.B. Iyer, S. Srinivas, Thin Solid Films 305 (1997) 259.

[40] G. Sánchez, W.L. Wang, M.C. Polo, J. Esteve, Diamond Relat. Mater. 7 (1998) 200.

[41] M. Chiang, M. Hon, J. Cryst. Growth 211 (2000) 211.

[42] K.V. Ravi, C.A. Koch, H.S. Hu, A. Joshi, J. Mater. Res. 5 (1990) 2356.

[43] D. Michau, B. Tanguy, G. Demazeau, M. Couzi, R. Cavagnat, Diamond Relat. Mater. 2 (1993) 19.

[44] Z. Li, L. Wang, T. Suzuki, A. Argoitia, P. Pirouz, J. Angus, J. Appl. Phys. 73 (1993) 711.

[45] J.A. Baglio, B.C. Fransworth, S. Hankin, C. Sung, J. Hefter, M. Tabasky, in: R.E. Clausing, L.L. Horton, J.C. Angus, P. Koidl (Eds.), Diamond and Diamond-like Films and Coatings, Plenum Press, New York, 1991, p. 635.

[46] P. Mahalingam, D.S. Dandy, Thin Solid Films 322 (1998) 108.

[47] R. Haubner, B. Lux, Diamond Relat. Mater. 2 (1993) 1277.

[48] J. Graul, E. Wagner, Appl. Phys. Lett. 21 (1972) 67.

[49] C.J. Magab, H.J. Leamy, J. Appl. Phys. 45 (1974) 1075.

[50] A.J. Steckl, J.P. Li, Thin Solid Films 216 (1992) 149.

[51] J.P. Li, A.J. Steckl, I. Golecki, F. Reidinger, L. Wang, X.J. Ning, P. Piroux, Appl. Phys. Lett. 62 (1993) 3135.

[52] J.P. Li, A.J. Steckl, J. Electrochem. Soc. 142 (1995) 634.

[53] B. Bahavar, M.I. Chaudhry, R.J. Mccluskey, Appl. Phys. Lett. 63 (1993) 914.

[54] N. Bécourt, J.L. Ponthenier, A.M. Papon, C. Jaussaud, Physica. B 185 (1993) 79.

[55] G. Ferro, Y. Monteil, H. Vincent, V. Thevenot, M.D. Tran, F. Cauwet, J. Bouix, J. Appl. Phys. 80 (1996) 4691.

[56] G. Ferro, Y. Monteil, H. Vincent, F. Cauwet, J. Bouix, P. Durupt, J. Olivier, R. Bisaro, Thin Solid Films 278 (1996) 22.

[57] V. Cimalla, J. Pezoldt, G. Ecke, G. Eichhorn, Inst. Phys. Conf. Ser. 142 (1996) 153.

[58] H. Romanus, V. Cimalla, A. Kromka, J. Scheiner, L. Spiess, J. Pezoldt, Mater. Sci. Eng., B, Solid-state Mater. Adv. Technol. 47 (1997) 274.

[59] C. Bittencourt, M. De Seta, F. Evangelisti, J. Vac. Sci. Technol., B 16 (1998) 1599.

[60] C.A. Zorman, S. Roy, C.H. Wu, A.J. Fleischman, M. Mehregany, J. Mater. Res. 13 (1998) 406.

[61] C.D. Stinespring, J.C. Wormhoudt, J. Appl. Phys. 45 (1974) 1075.

[62] M. Tomellini, R. Polini, V. Sessa, J. Appl. Phys. 70 (1991) 7573.

[63] E. Molinari, R. Polini, M.L. Terranova, P. Ascarelli, S. Fontana, J. Mater. Res. 7 (1992) 1778.

[64] E. Molinari, R. Polini, V. Sessa, M.L. Terranova, M. Tomellini, J. Mater. Res. 8 (1993) 785.

[65] E. Molinari, R. Polini, M. Tomellini, J. Mater. Res. 8 (1993) 798.

[66] M. Tomellini, J. Mater. Res. 8 (1993) 1596.

[67] H. Liu, D.S. Dandy, J. Electrochem. Soc. 143 (1996) 1104.

[68] M.H. Hon, R.F. Davis, J. Mater. Sci. 14 (1979) 2411.

[69] J.A. Venables, Philos. Mag. 27 (1973) 697.

[70] P. Mahalingam, H. Liu, D.S. Dandy, J. Appl. Phys. 81 (1997) 1966.

[71] M. Ohring, The Materials Science of Thin Films, 1992. Academic Press, Harcourt Brace Jovanovich Pub., Boston, MA.

[72] M.E. Coltrin, R.J. Kee, G.H. Evans, E. Meeks, F.H. Rupley, J.F. Grear, Report No. SAND 91-8003 (1991).

[73] R.J. Kee, F.M. Rupley, J.A. Miller, Report No. SAND 89-8009B (1993).

[74] M.E. Coltrin, R.J. Kee, F.M. Rupley, Report No. SAND 90-8003B (1991).

[75] R.J. Kee, G. Dixon-Lewis, J. Warnatz, M.E. Coltrin, J.A. Miller, Report No. SAND 86-8246 (1986).

[76] M.E. Coltrin, D.S. Dandy, J. Appl. Phys. 74 (1993) 5803.

[77] C.C. Battaile, D.J. Srolovitz, I.I. Oleinik, D.G. Pettifor, A.P. Sutton, S.J. Harris, J.E. Butler, J. Chem. Phys. 111 (1999) 4291.

[78] M.D. Allendorf, R.J. Kee, J. Electrochem. Soc. 138 (1991) 841.

[79] R.B. Jackman, L.H. Chua, J.S. Ford, Surf. Sci. 292 (1993) 47.

[80] K. Feng, Z.H. Liu, Z. Lin, Surf. Sci. 329 (1995) 77.

[81] A.J. Dyson, P.V. Smith, Surf. Sci. 396 (1998) 24.

[82] J.A. Venables, G.D.T. Spiller, M. Hanbücken, Rep. Prog. Phys. 47 (1984) 399.

[83] B. Lewis, Thin Solid Films 1 (1967) 85.

[84] G. Zinsmeister, Thin Solid Films 4 (1969) 363.

[85] B. Lewis, D.S. Campbell, J. Vac. Sci. Technol. 4 (1967) 209.

[86] J.C. Fisher, J. Appl. Phys. 22 (1951) 74.

[87] T. Suzuoka, J. Phys. Soc. Jpn. 19 (1964) 839.

[88] J. Crank, The Mathematics of Diffusion, 1975. Oxford University Press, Ely House, London, UK.

[89] C. Wild, N. Herres, P. Koidl, J. Appl. Phys. 68 (1990) 973.

[90] C. Wild, P. Koidl, W. Muller-Sebert, H. Walcher, R. Kohl, N. Herres, R. Locher, R. Samlenski, R. Brenn, Diamond Relat. Mater. 2 (1993) 158.

[91] D.J. Srolovitz, D.S. Dandy, J.E. Bulter, C.C. Battaile, F. Paritosh, JOM 49 (1997) 42.

[92] D.S. Dandy, M.E. Coltrin, J. Appl. Phys. 76 (1994) 3102.

[93] Y.S. Cheng, C.H. Sho, G.F. Shu, J. Cryst. Growth 99 (1990) 1196.

[94] J.W. Kim, Y.J. Baik, K.Y. Eun, in: Y. Tzeng, M. Yoshikawa, A. Feldman (Eds.), Applications of Diamond Films and Related Materials, Elsevier Science Pub., Amsterdam, 1991, p. 399.